Supplemental information

Deletion of IRS-1 leads to growth failure and insulin resistance with downregulation of liver and muscle insulin signaling in rats

Yuka Toyoshima, Katsuyuki Nakamura, Yusuke Taguchi, Reiko Tokita, Shiho Takeuchi, Hayato Osawa, Naomi Teramoto, Hidetoshi Sugihara, Fumiaki Yoshizawa, Keitaro Yamanouchi, Shiro Minami

Supplemental Table S1

The body weight, body length, and tissue weights of WT and KO rats at 15 weeks of age.

	Male		Female	
	WT	**KO**	**WT**	**KO**
	n = 8	**n = 12**	**n = 10**	**n = 11**
Body weight, g	479 ± 43	189 ± 11*	280 ± 17	132 ± 12*
Liver weight, g	15.5 ± 1.9	6.4 ± 0.4*	10.2 ± 0.9	5.6 ± 0.5*
Gastrocnemius muscle weight, g	5.0 ± 0.3	1.6 ± 0.1*	3.1 ± 0.2	1.2 ± 0.1*
Kidney weight, g	3.4 ± 0.3	2.0 ± 0.1*	2.0 ± 0.1	1.3 ± 0.1*
Brain weight, g	1.9 ± 0.1	1.5 ± 0.1*	1.7 ± 0.1	1.4 ± 0.1*
Epidydimal fat pad weight, g	4.9 ± 1.2	2.8 ± 0.5*	-	-

Values are means ± SDs. * $p<0.05$ vs. WT rats.

Supplemental Table S2

The blood glucose, plasma insulin, serum triglyceride (TG), and serum non-esterified fatty acids (NEFA) levels of WT and KO rats at 15 weeks of age.

	Male		Female	
	WT	**KO**	**WT**	**KO**
	n = 8	**n = 13**	**n = 12**	**n = 13**
Blood glucose level, mg/dL	123 ± 6	114 ± 12	129 ± 9	126 ± 11
Plasma insulin level, ng/mL	8.3 ± 3.0	14.3 ± 8.8*	5.3 ± 3.5	11.2 ± 6.8*
Serum TG level, mg/dL	55 ± 14	49 ± 8	65 ± 10	71 ± 11
Serum NEFA level, mEq/L	0.47 ± 0.08	0.77 ± 0.15*	0.36 ± 0.06	0.58 ± 0.13*

Values are means ± SDs. * $p<0.05$ vs. WT rats.

Supplemental Figure S1

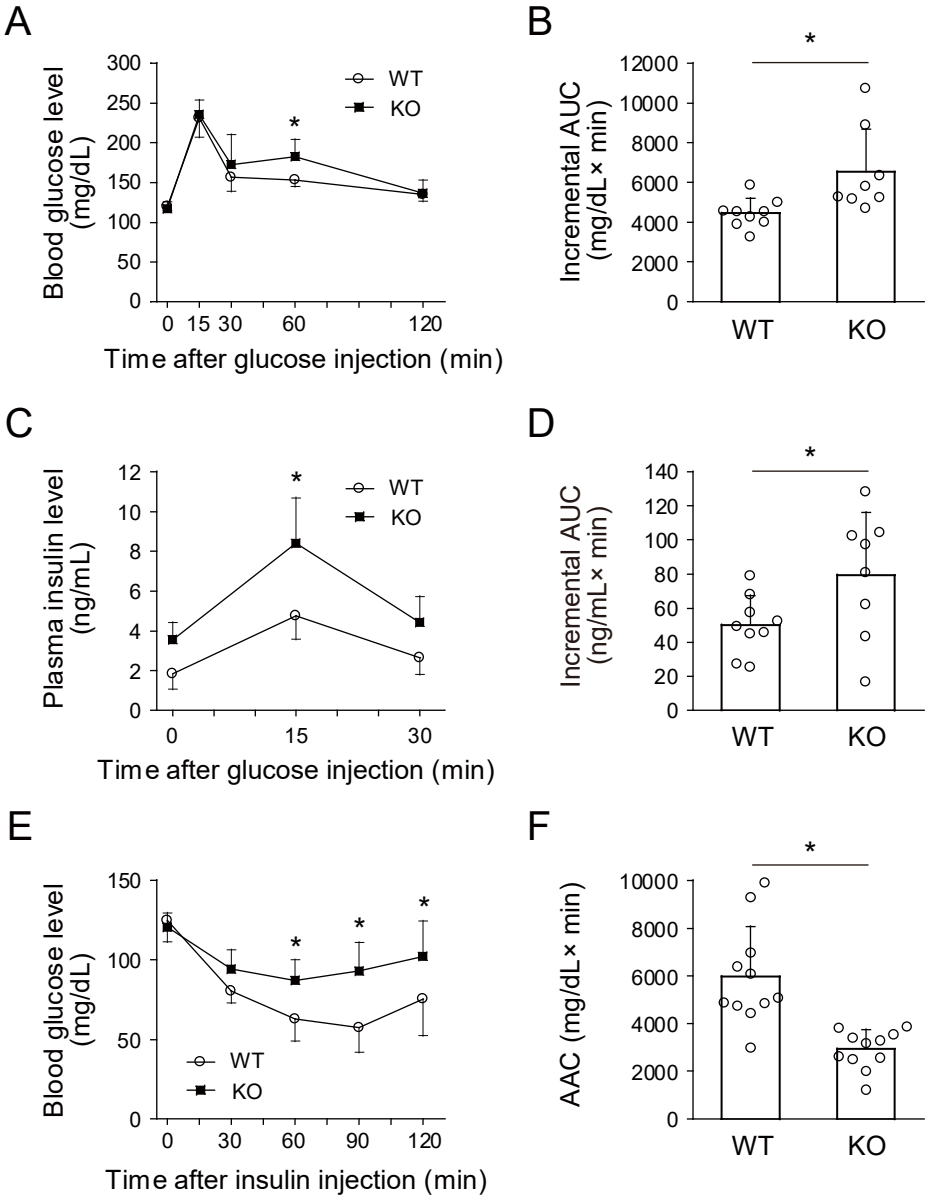

Fig. S1. Glucose tolerance test (GTT) and insulin tolerance test (ITT) in female WT and IRS-1 KO rats.
A–D: The GTT results for the WT (n=9) and KO (n=8) rats at 12 weeks of age. A: Changes in the blood glucose levels during the GTT. B: The incremental AUC for the blood glucose level during the GTT. C: Changes in plasma insulin levels during the GTT. D: The incremental AUC for the plasma insulin level during the GTT. E, F: The ITT results for the WT (n=11) and KO (n=11) rats at 13 weeks of age. E: Changes in the blood glucose levels during the ITT. F: The area above the curve (AAC) for the blood glucose level during the ITT. Values are means ± SDs. *$p<0.05$ vs. WT rats.

Supplemental Figure S2

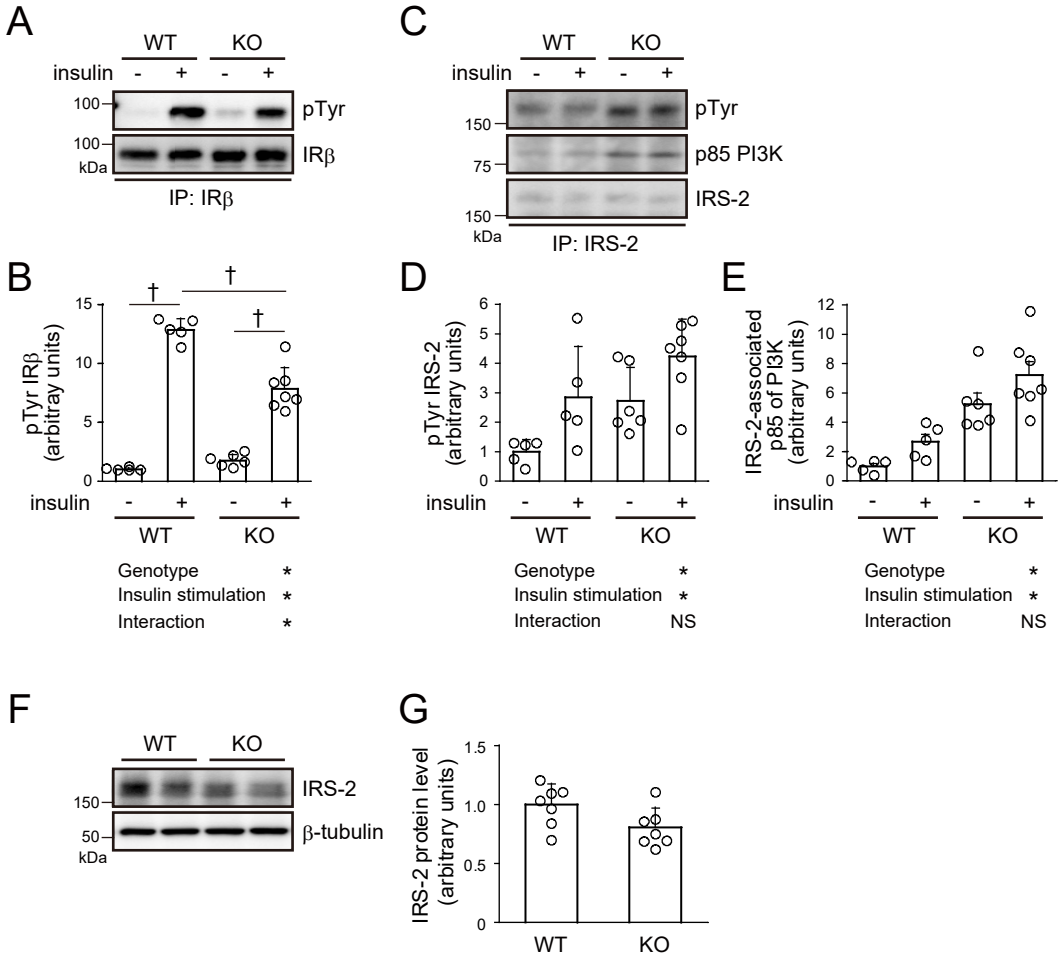

Fig. S2. The insulin-stimulated phosphorylation of IRβ and IRS-2 and the amount of IRS-2 protein in the white adipose tissue (WAT) of WT and IRS-1 KO rats. Eight-week-old male WT and KO rats were fasted overnight, and insulin or vehicle was subsequently injected into the inferior vena cava. A-E: The epididymal WAT was dissected at 2 min after the insulin injection. A, B: Insulin-stimulated tyrosine phosphorylation of IRβ. The immunoprecipitated IRβ from the homogenates was analyzed by immunoblotting with anti-phosphotyrosine (pTyr) and anti-IRβ antibodies. A: Representative immunoblots. B: The ratio of pTyr to the amount of immunoprecipitated IRβ. The immunoreactivity of pTyr was quantified and divided by the immunoreactivity of IRβ. C-E: Insulin-stimulated tyrosine phosphorylation of IRS-2 and its association with the p85 regulatory subunit of PI3K (p85 of PI3K). The immunoprecipitated IRS-2 from the homogenates was analyzed by immunoblotting with anti-pTyr, anti-p85 of PI3K, and anti-IRS-2 antibodies. C: Representative immunoblots. D: The ratio of pTyr to the amount of immunoprecipitated IRS-2. The immunoreactivity of pTyr was quantified and divided by the immunoreactivity of IRS-2. E: The ratio of p85 of PI3K to the amount of immunoprecipitated IRS-2. The immunoreactivity of p85 of PI3K was quantified and divided by the immunoreactivity of IRS-2. Values are means ± SDs. WT with −insulin group, n=5. WT with +insulin group, n=5. KO with −insulin group, n=6. KO with +insulin group, n=7. The results of two-way ANOVA are shown below the graph (*$p<0.05$, NS; not significant). The results of Tukey-Kramer post-hoc test are shown in the graph when there was a significant interaction of genotype and insulin stimulation (†$p<0.05$). F, G: The IRS-2 protein level of the vehicle-injected WT (n=7) and KO (n=7) rats. Total homogenates were analyzed by immunoblotting with antibodies against IRS-2 and β-tubulin. Values are means ± SDs. Similar results were obtained using the WAT homogemates prepared from the different set of animals.

Supplemental Figure S3

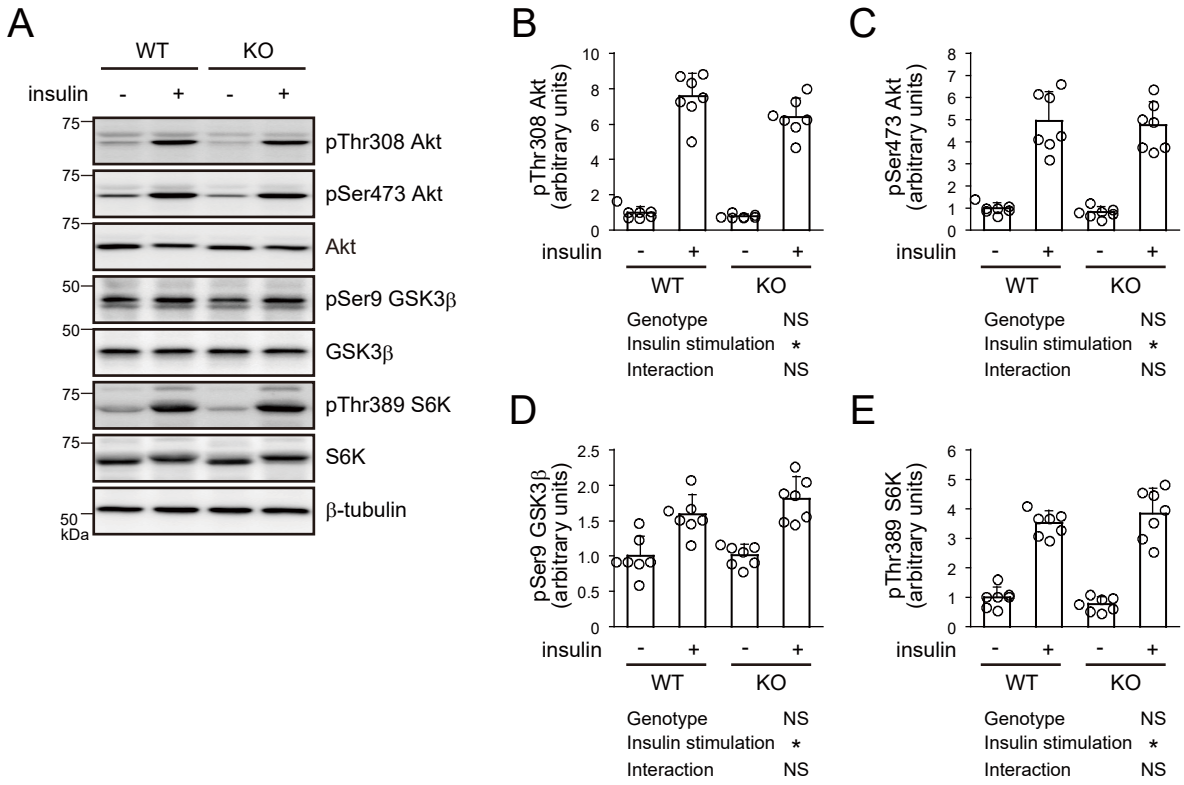

Fig. S3. The insulin-stimulated phosphorylation of Akt, GSK3β, and S6K in the white adipose tissue (WAT) of WT and IRS-1 KO rats. Eight-week-old male WT and KO rats were fasted overnight, and insulin or vehicle was subsequently injected into the inferior vena cava.The epididymal WAT was excised at 15 min after the insulin injection.

A–E: Insulin-stimulated phosphorylation of Akt, GSK3β, and S6K in the WAT. A: Representative immunoblots. B–E: The immunoreactivities of Thr308 phosphorylation of Akt (B), Ser473 phosphorylation of Akt (C), Ser9 phosphorylation of GSK3β (D), and Thr389 phosphorylation of S6K (E) were quantified and divided by the immunoreactivity of β-tubulin. Values are means ± SDs (n=7). Two-way ANOVA results are shown below the graph (*$p<0.05$, NS; not significant).

Supplemental Figure S4

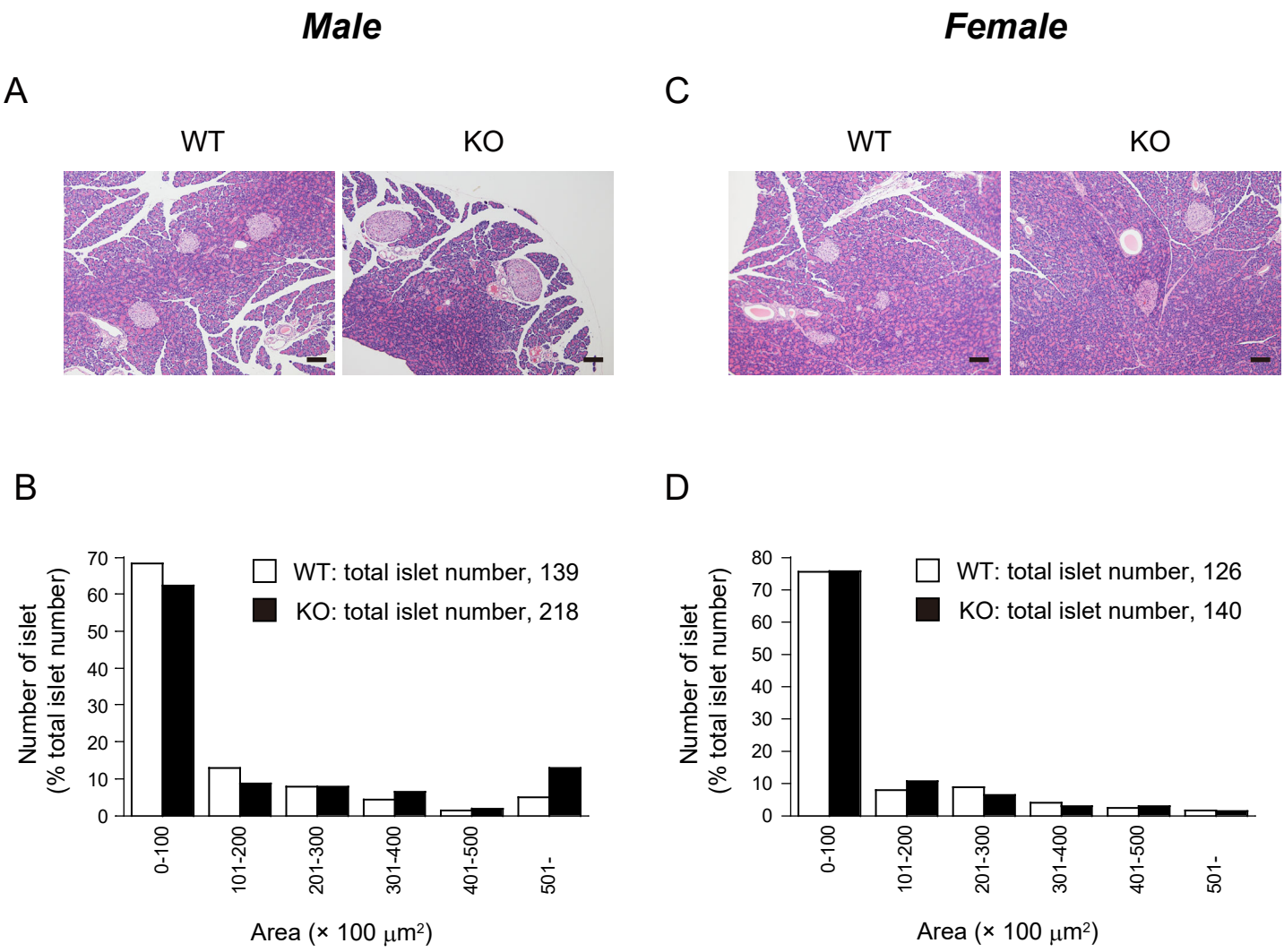

Fig. S4. The morphology of islets in 15-week-old WT and IRS-1 KO rats. The paraffine embedded sections of pancreatic islets were stained with hematoxylin and eosin. A, B: Representative sections (A) and the quantification of islet area (B) in 15-week-old male WT (n=5) and KO (n=5) rats. Total observed islet number in WT males was 139, and that in KO males was 218. The average of islet area in WT males was 116 × 100 μm², and that in KO males was 211 × 100 μm². B, C: Representative sections (A) and the quantification of islet area (B) in 15-week-old female WT (n=5) and KO (n=5) rats. Total observed islet number in WT females was 126, and that in KO males was 140. The average of islet area in WT males was 86 × 100 μm², and that in KO males was 84 × 100 μm². Images are shown as 10× magnification; the bar represents 100 μm.

Supplemental Figure S5

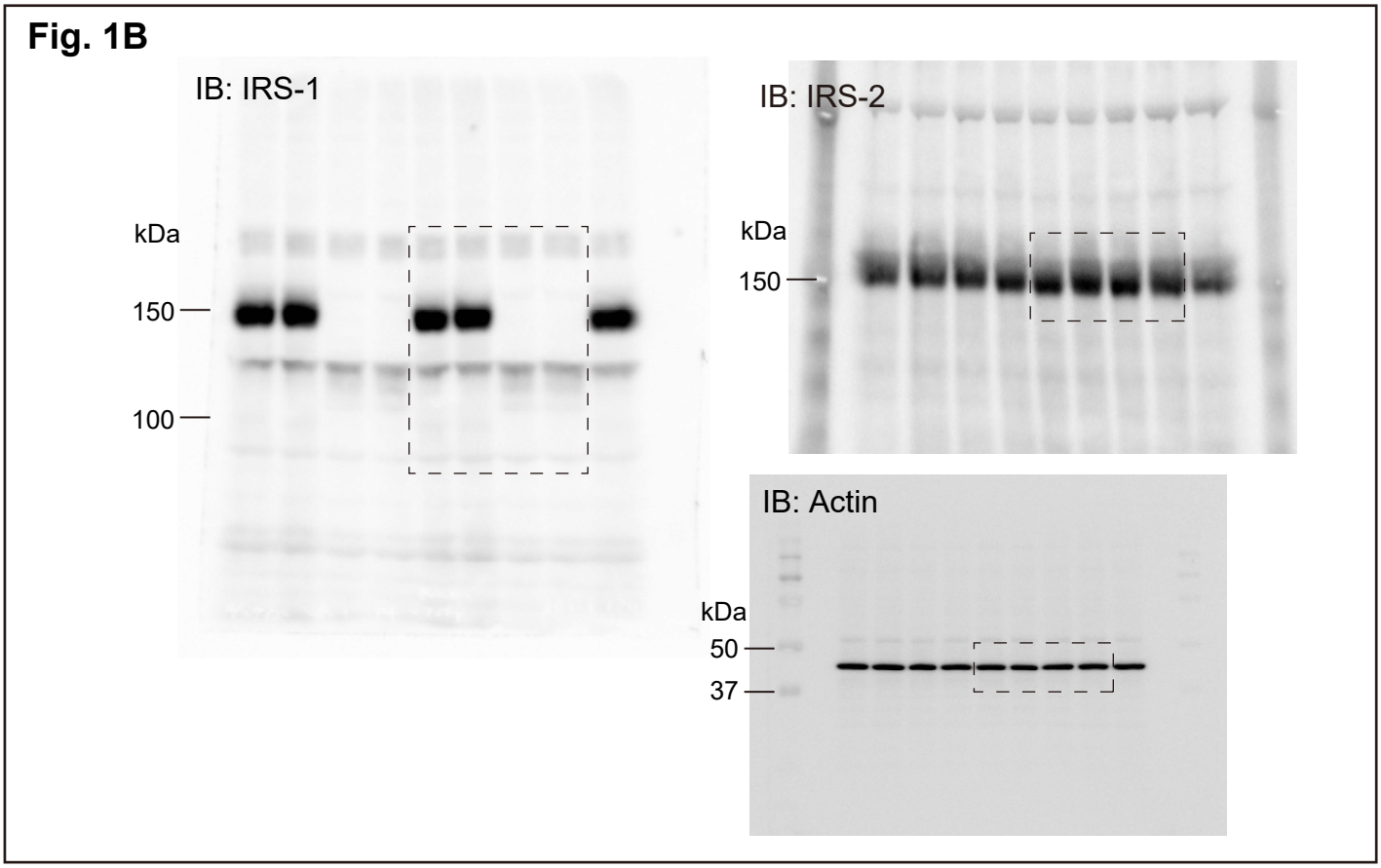

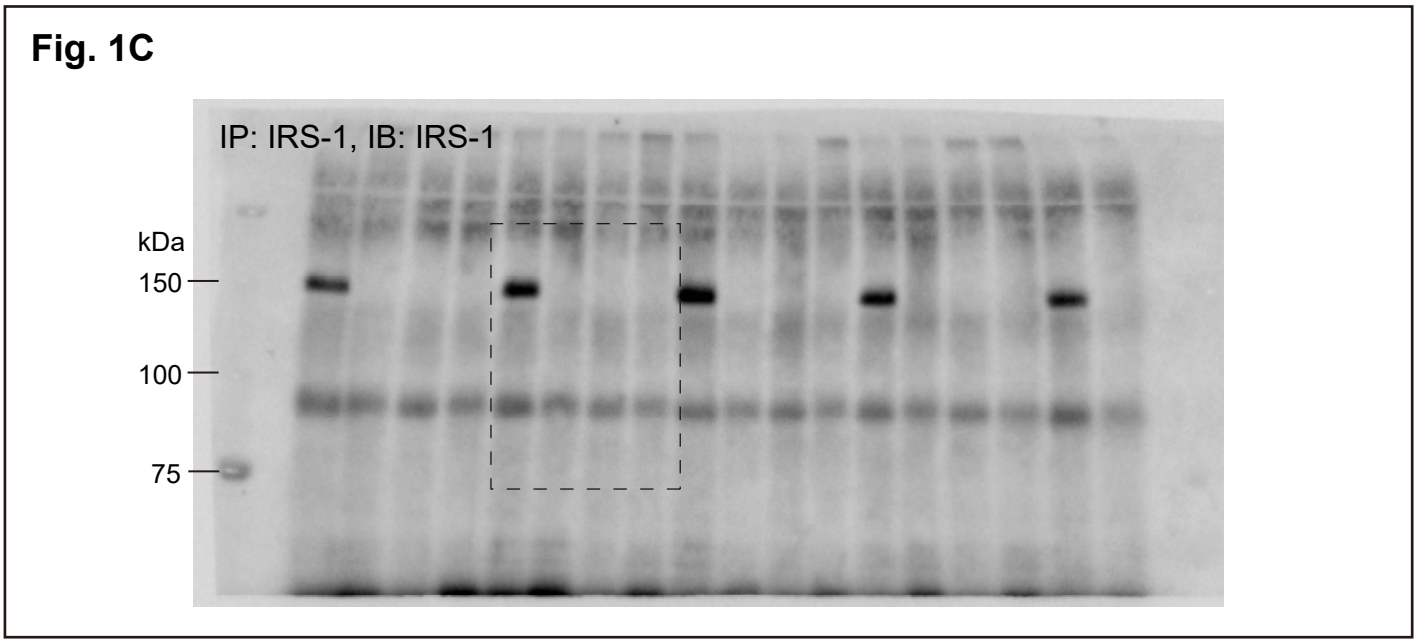

Fig. S5. The unprocessed blots shown in Fig. 1B and 1C.
The dotted rectangles delimit cropped areas used in Fig.1.

Supplemental Figure S6

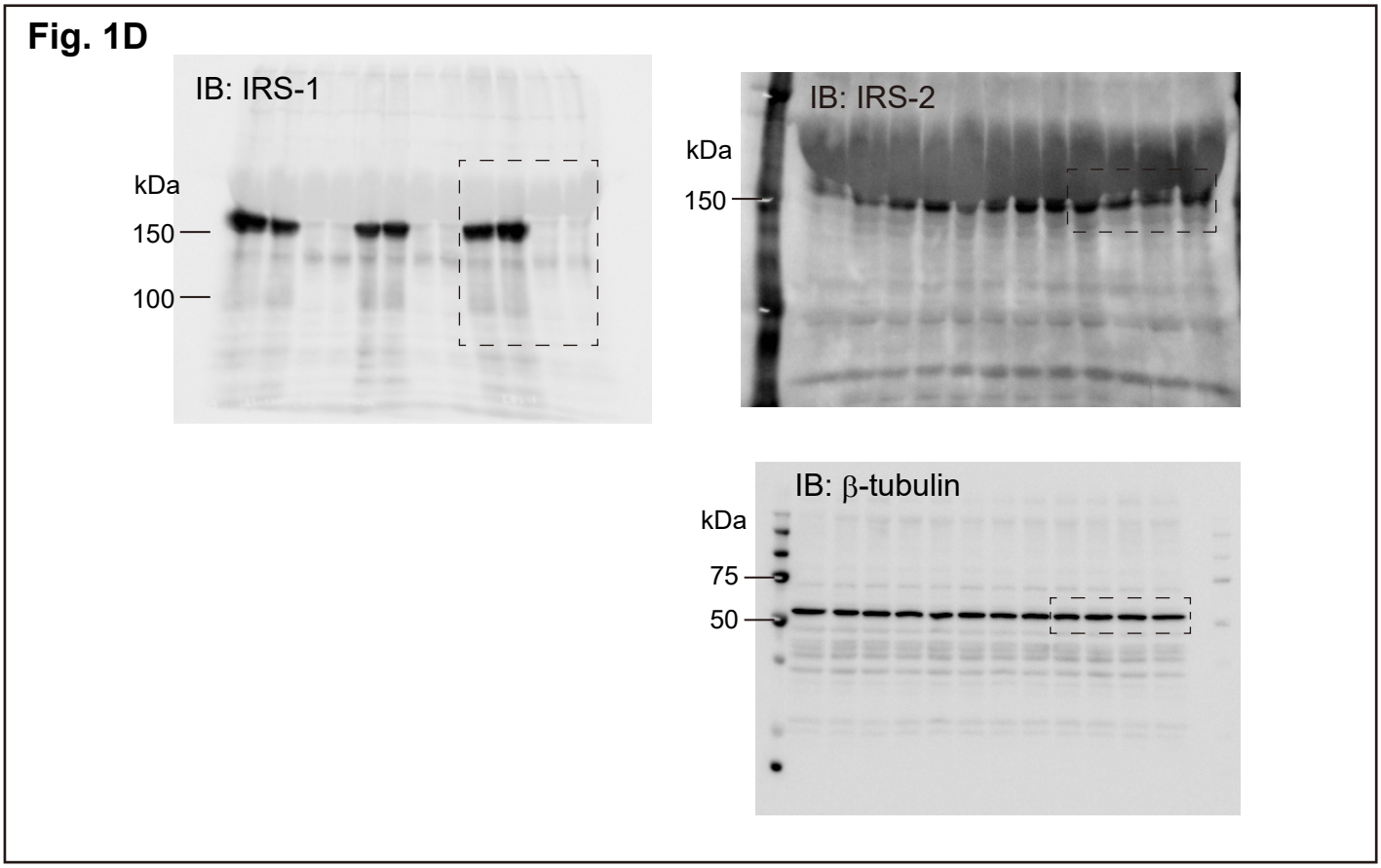

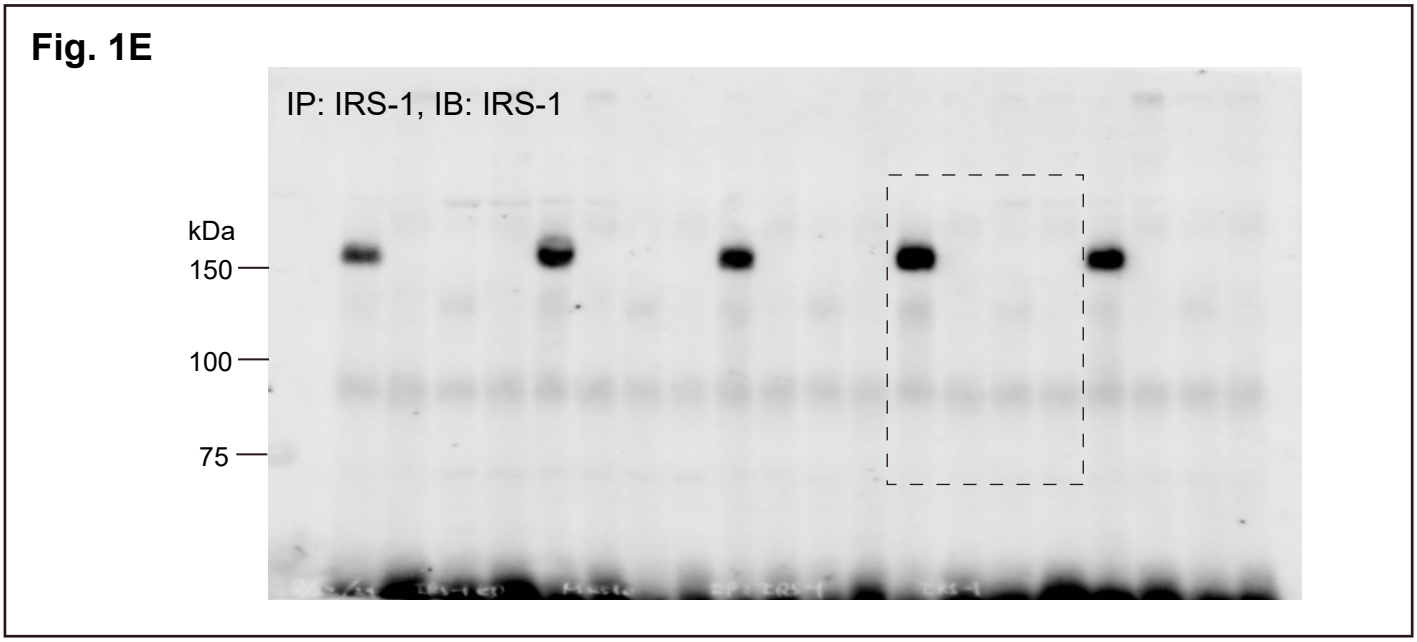

Fig. S6. The unprocessed blots shown in Fig. 1D and 1E.
The dotted rectangles delimit cropped areas used in Fig.1.

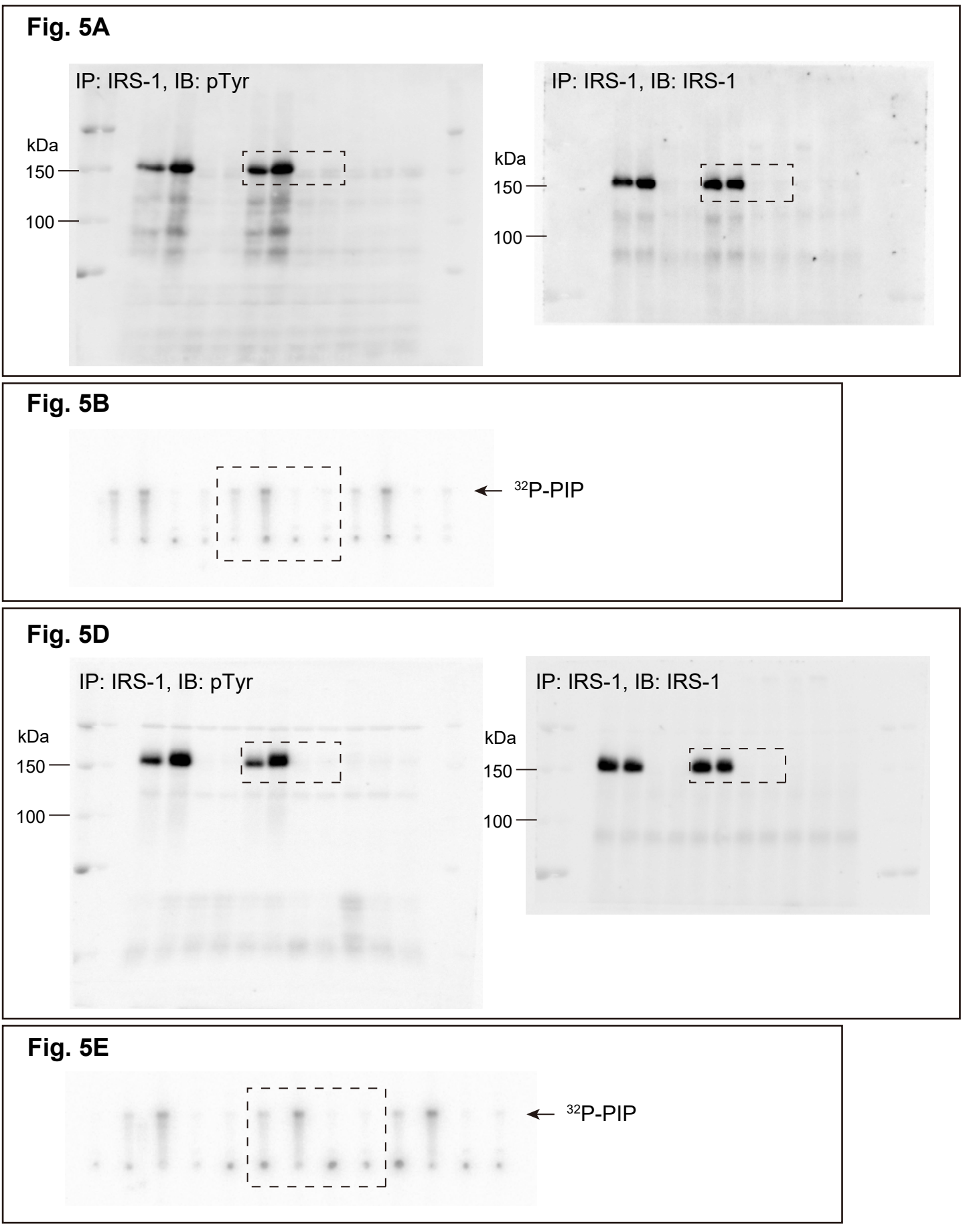

Fig. S7. The unprocessed blots shown in Fig. 5A, 5B, 5D, and 5E.
The dotted rectangles delimit cropped areas used in Fig.5.

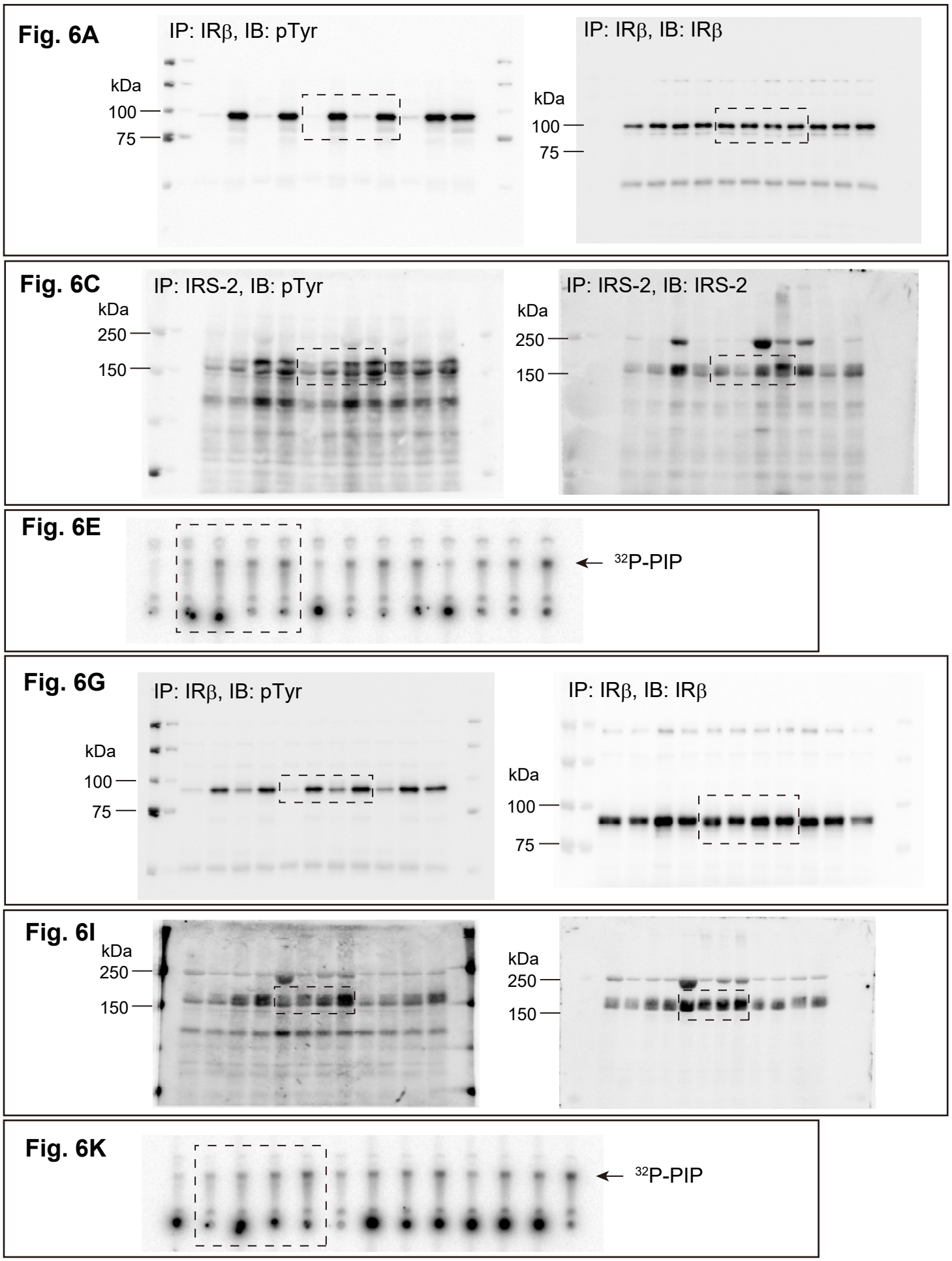

Fig. S8. The unprocessed blots shown in Fig. 6A, 6C, 6E, 6G, 6I, and 6K.
The dotted rectangles delimit cropped areas used in Fig.6.

Supplemental Figure S9

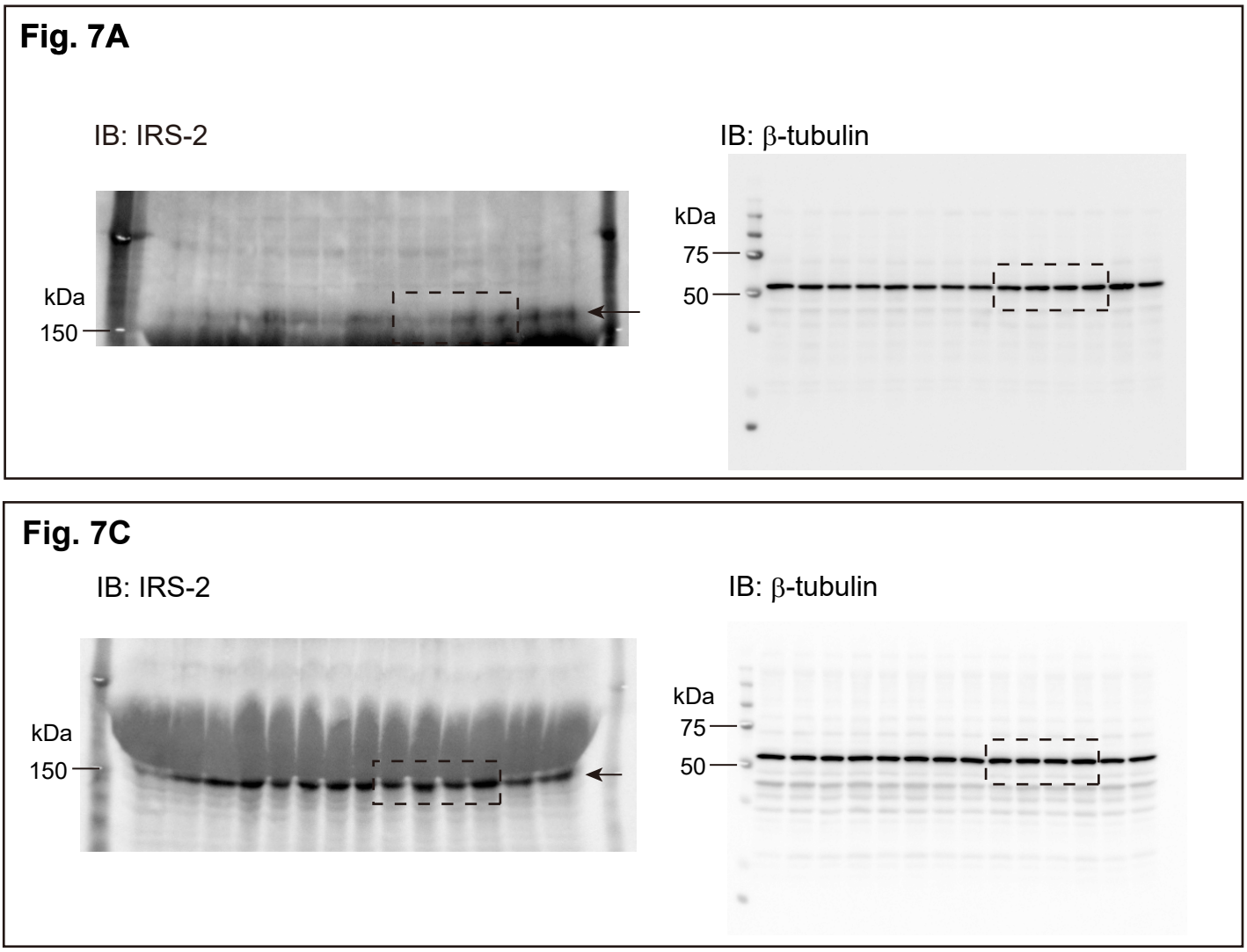

Fig. S9. The unprocessed blots shown in Fig. 7A and 7C.
The dotted rectangles delimit cropped areas used in Fig.7.

Supplemental Figure S10

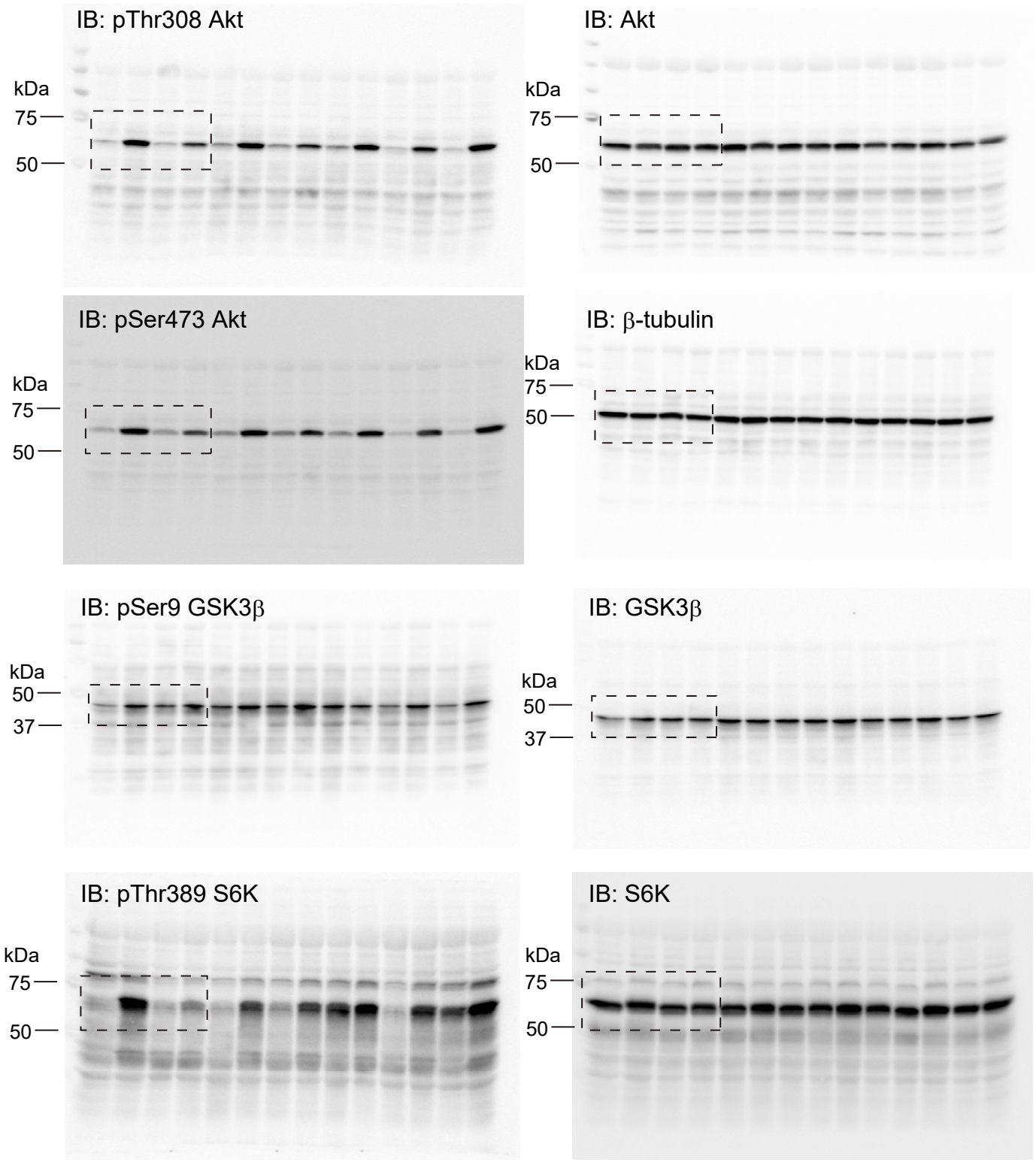

Fig. S10. The unprocessed blots shown in Fig. 8A.
The dotted rectangles delimit cropped areas used in Fig.8.

Supplemental Figure S11

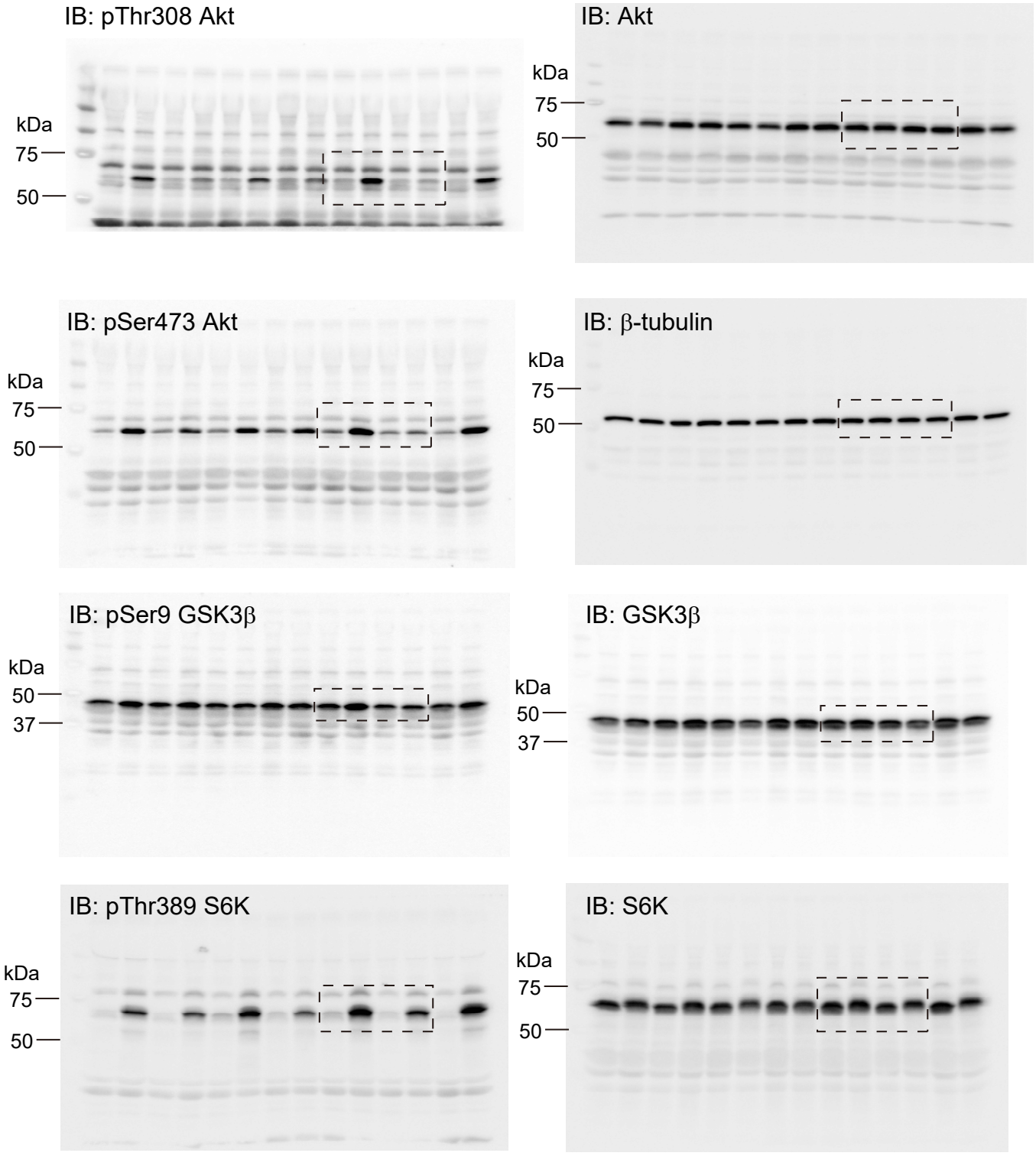

Fig. S11. The unprocessed blots shown in Fig. 8F.
The dotted rectangles delimit cropped areas used in Fig.8.

Fig. S2A

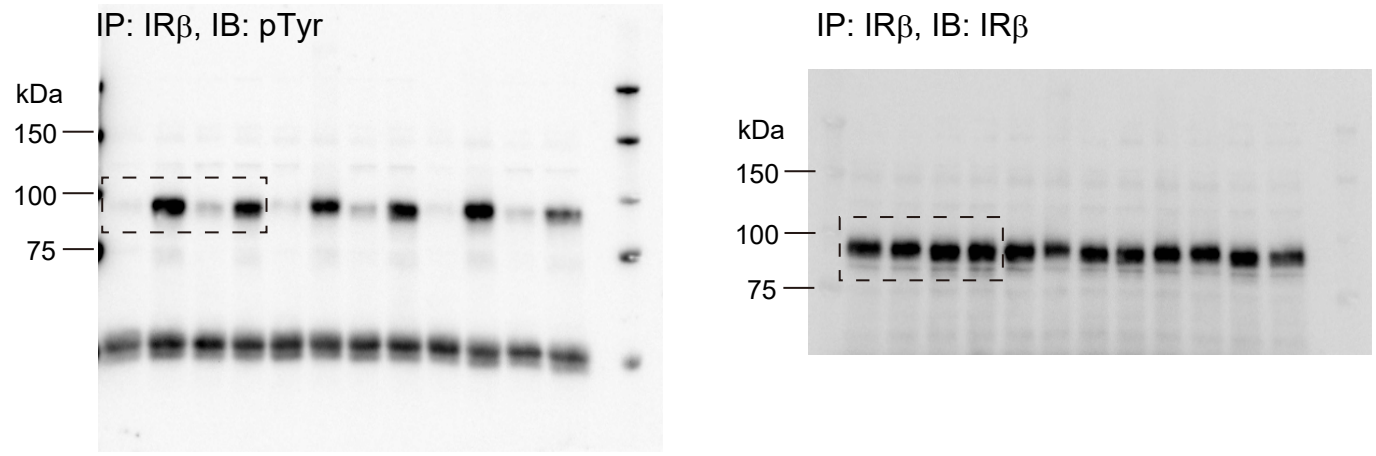

Fig. S2C

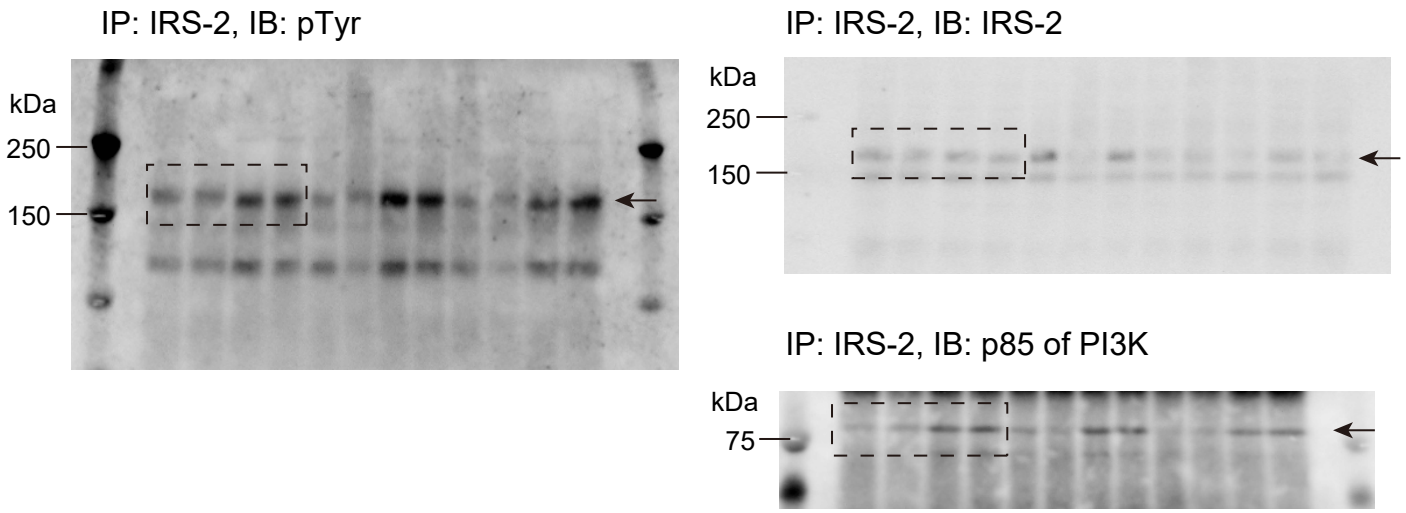

Fig. S2F

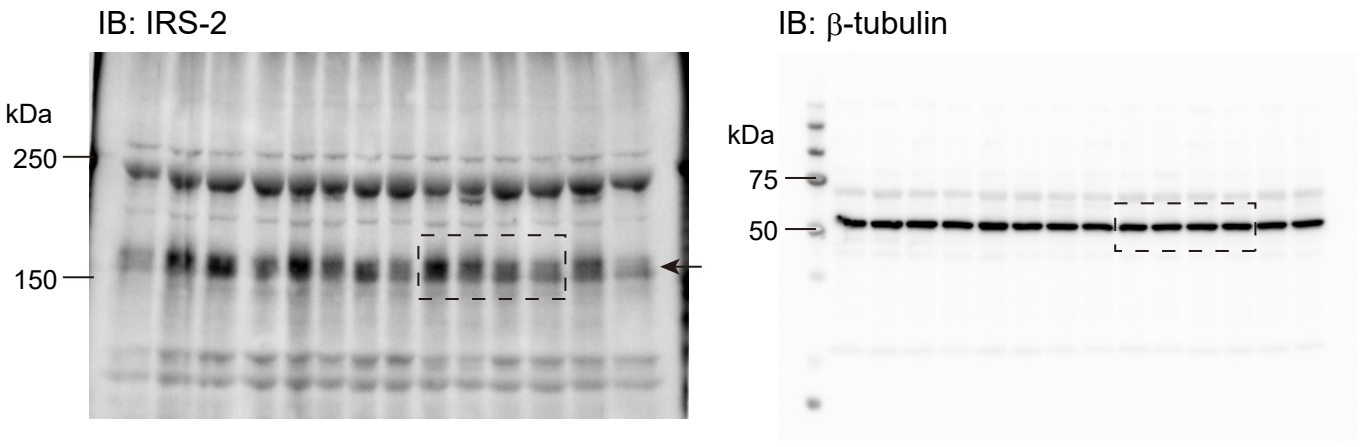

Fig. S12. The unprocessed blots shown in Fig. S2A, 2C, and 2F.
The dotted rectangles delimit cropped areas used in Fig.S2.

Supplemental Figure S13

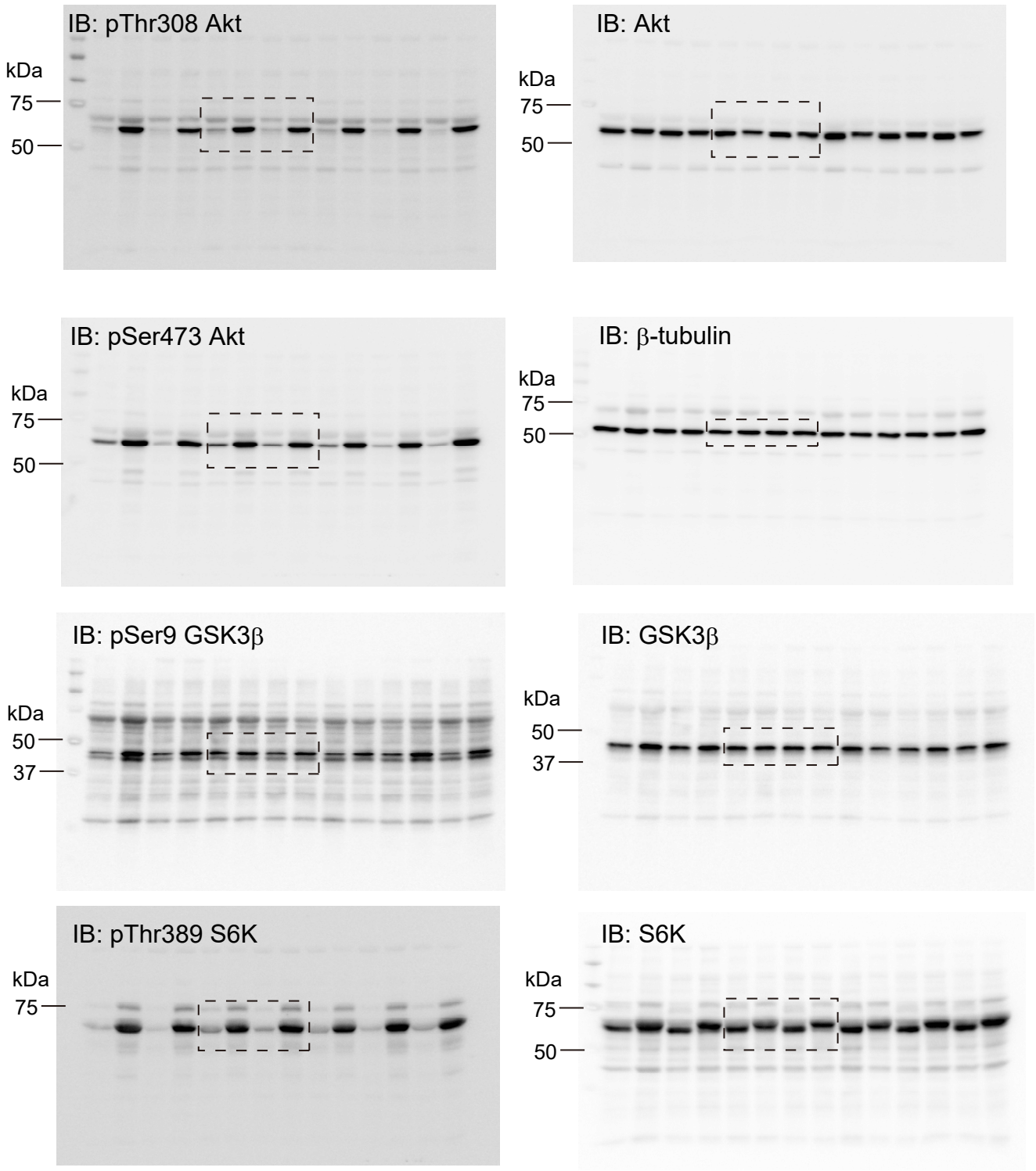

Fig. S13. The unprocessed blots shown in Fig. S3A.
The dotted rectangles delimit cropped areas used in Fig. S3.